Clim. Past Discuss., 11, 5203–5241, 2015
www.clim-past-discuss.net/11/5203/2015/
doi:10.5194/cpd-11-5203-2015

Climate of the Past Discussions
Open Access
EGU

The impact of the North American ice sheet on the evolution of the Eurasian ice sheet during the last glacial cycle

J. Liakka[1], M. Löfverström[2], and F. Colleoni[3]

[1]Biodiversity and Climate Research Centre, Senckenberg Gesellschaft für Naturforschung, Senckenberganlage 25, 60325 Frankfurt am Main, Germany
[2]National Center for Atmospheric Research, 1850 Table Mesa Drive, 80305 Boulder, CO, USA
[3]Centro Euro-Mediterraneo sui Cambiamenti Climatici, via Franceschini 31, 40128 Bologna, Italy

Received: 9 October 2015 – Accepted: 25 October 2015 – Published: 10 November 2015

Correspondence to: J. Liakka (johan.liakka@senckenberg.de)

Published by Copernicus Publications on behalf of the European Geosciences Union.

Abstract

Modeling studies show that the massive ice sheet expanding over the North American and Eurasian continents in the last glacial cycle has a large impact on the atmospheric stationary waves and thus yielded a glacial climate distinctly different from the present. However, to what extent the two ice sheets influenced each others growth trajectories remains largely unexplored. In this study we investigate how ice sheets in North America influence the downstream evolution of the Eurasian ice sheet, using a thermomechanical ice-sheet model forced by climate data from snapshot simulations of three distinctly different phases of the last glacial cycle: the Marine Isotope Stages 5b, 4 and 2 (LGM). Our results suggest that changes in the North American paleo-topography may have had a large influence on evolution of the Eurasian ice sheet. In the MIS4 and LGM experiments, the Eurasian ice sheet migrates westward towards the Atlantic sector – largely consistent with geological data and contemporary ice-sheet reconstructions – due to a low wavenumber stationary wave response, which yields a cooling in Europe and a warming in northeastern Siberia. The expansion of the North American ice sheet between MIS4 and LGM amplifies the Siberian warm anomaly, which limits the glaciation there and may therefore help to explain the progressive westward migration of the Eurasian ice sheet over this time period. While the Eurasian ice sheet in the MIS4 and LGM experiments appears to be in equilibrium with the simulated climate conditions, the MIS5b climate forcing is too warm to grow an ice sheet. First-order sensitivity experiments suggest that most of the MIS5b ice sheet was established during preceding colder stages.

1 Introduction

The Quaternary period is characterized by the alternation between cold and warm phases – glacial and interglacials – when massive ice sheets expand and retreat over the subpolar continents. The last glacial cycle began about 115 000 years ago (115 kyrs

CPD
11, 5203–5241, 2015

BP) following a minimum in the boreal summer insolation (Berger and Loutre, 1991). Over the subsequent ∼ 90 kyrs, paleo-records suggest that ice sheets progressively expanded in North America and Eurasia, with periods of relatively rapid ice growth during colder phases (stadials) followed by warmer periods (interstadials) when global ice volume remained relatively constant (Peltier and Fairbanks, 2006; Stokes et al., 2012; Kleman et al., 2013). The stadials are referred to as the Marine Isotope Stages (MIS) 5d (106–115 kyrs BP), 5b (85–93 kyrs BP), 4 (60–74 kyrs BP) and 2 (12–24 kyrs BP), where the latter includes the culmination of the last glacial cycle at the Last Glacial Maximum (LGM; 19–23 kyrs BP).

The progressive increase of the Northern Hemisphere ice volume was dominated by the Laurentide and Cordilleran ice sheets in North America (Kleman et al., 2013). Subsequent to the ice-sheet inception in the Canadian Arctic and Quebec, the Laurentide ice sheet expanded over the eastern parts of the continent and eventually coalesced with the Cordilleran ice sheet to form a coherent continent-wide ice sheet at the LGM (Fig. 1; Clark et al., 1993; Kleman et al., 2010, 2013). As opposed to the North American counterpart, the combined volume of the Eurasian ice sheets (Fennoscandian and Barents-Kara ice sheets) changed relatively little between the inception phase and LGM (Fig. 1; Svendsen et al., 2004; Kleman et al., 2013). Instead, the most notable feature of the ice-sheet evolution in Eurasia is a progressive westward migration in time; in the early and intermediate stages (MIS5b and MIS4) the eastern margin of the Eurasian ice sheet was located in central Siberia (Svendsen et al., 2004; Kleman et al., 2013), whereas essentially only northern Europe and the British Isles (Bradwell et al., 2008) were ice covered at the LGM (Fig. 1). Hence, in both the North American and Eurasian continents, the ice sheets had strong zonal asymmetries toward the Atlantic sector over large parts of the glacial cycle. The driving mechanism of this asymmetry remains an open question as it has been difficult to capture this feature in conventional ice-sheet model experiments (Marshall et al., 2000; Zweck and Huybrechts, 2005; Charbit et al., 2007; Bonelli et al., 2009; Beghin et al., 2014).

CPD
11, 5203–5241, 2015

The role of ice sheet-atmosphere interactions has mostly been studied for build-up of the ice sheets in North America. These studies suggest that the east-heavy pre-LGM configuration arose from changes in the time-mean atmospheric circulation (stationary waves) forced by the ice sheet itself, possibly in combination with complex interactions with the North American Cordillera (Roe and Lindzen, 2001; Liakka et al., 2011; Löfverström et al., 2014, 2015). The mechanisms behind the temporal evolution of the Eurasian ice sheet have received less attention. The orographic precipitation feedback, initially proposed by Sanberg and Oerlemans (1983), is generally considered an important feature to explain the westward migration of the ice sheet (Roe and Lindzen, 2001; Van Den Berg et al., 2008; Liakka and Nilsson, 2010; Kleman et al., 2013; Löfverström et al., 2014). Surface winds from the Atlantic are forced vertically by the western and southern slopes of the ice sheet, hence leading to increased precipitation rates in those regions and ultimately to a (south)westward propagation of the ice sheet (Sanberg and Oerlemans, 1983). Although orographic precipitation is a robust feature in moist atmospheric circulation models (Roe, 2005), questions regarding the timing of the westward migration of the Eurasian ice sheet remain unanswered. For example, why did the Eurasian ice sheet propagate westward only in the later stages of glacial cycle and not immediately subsequent to the inception phase? The answer to this question is complicated by the fact that the orientation of the Atlantic storm track, which has a large impact on the European precipitation, appears to be controlled by the size of the North American ice sheet; for smaller ice sheets in North America (e.g. MIS5b and MIS4) the Atlantic storm track has a pronounced southwest-northeast tilt (similar to the modern climate), whereas for large ice sheets (LGM) the storm track has a more zonal orientation (Li and Battisti, 2008; Kageyama et al., 2013; Löfverström et al., 2014; Ullman et al., 2014; Merz et al., 2015). The zonalisation of the Atlantic storm track typically yields drier (wetter) conditions in northern (southern) Europe (Löfverström et al., 2014).

The connection between the size of the Laurentide ice sheet and the orientation of the Atlantic storm track suggests that the ice sheets in North America may have influ-

CPD
11, 5203–5241, 2015

enced the ice sheet evolution in Eurasia. Studies investigating remote climate impacts of the North American and Eurasian paleo-topography typically use static ice sheets as forcing in comprehensive circulation models (e.g. Li and Battisti, 2008; Löfverström et al., 2014; Ullman et al., 2014) or dynamic ice sheet models coupled to highly simplified atmospheric models (sometimes with parameterized climate anomalies Beghin et al., 2014). In this study, we investigate the effect of the geologically-constrained ice sheets in North America at MIS5b, MIS4 and LGM (see Fig. 1) on the evolution of the Eurasian ice sheet. The atmospheric response to the North American ice sheets is evaluated using a comprehensive atmospheric circulation model with nonlinear dynamics (NCAR CAM3). The atmospheric fields are subsequently used as forcing in a thermomechanical ice-sheet model (SICOPOLIS) in order to evaluate their impact on the Eurasian ice sheet. More information about the models and the experiments is given in Sect. 2. In Sect. 3 we show the main results from the atmospheric and ice-sheet model experiments, followed by a comprehensive discussion in Sect. 4. Finally, the conclusions are summarized in Sect. 5.

2 Models and experiments

2.1 Atmospheric simulations

We use the climate snapshot (steady-state) simulations from Löfverström et al. (2014) representative for the MIS5b (88 kyrs BP), MIS4 (66 kyrs BP) and LGM (20 kyrs BP) climates. These experiments were conducted with the National Center for Atmospheric Research Community Atmospheric Model version 3 (NCAR CAM3; Collins et al., 2006) using T85 spectral resolution (approximately 1.4° horizontal resolution) and 26 hybrid levels in the vertical. Ice sheets and other land surface processes are handled by the Community Land Model 3 (CLM3; Oleson et al., 2004). The ocean surface is represented by a mixed-layer (slab) ocean model with a prescribed mixed-layer depth and ocean heat transport.

CPD
11, 5203–5241, 2015

For each glacial time slice, two sets of surface orography were used: (i) the reconstructed glacial orography from Kleman et al. (2013) (hereafter referred to as the "fullGlacial" simulations; see Fig. 1), and (ii) the present-day orography ("PDoro"). Each fullGlacial and PDoro simulation were carried out twice using two end-member representations of the ocean heat transport (OHT). Both OHT representations were derived from equilibrated simulations with the (NCAR) Community Climate System Model version 3 (CCSM3), which is a fully-coupled model using CAM3 as atmospheric component. The first OHT representation was derived from a pre-industrial simulation (hereafter referred to as "PI OHT"), and the second set from the LGM simulation in Brandefelt and Otto-Bliesner (2009) ("LGM OHT"). The simulations using LGM OHT yield an unrealistically extensive sea-ice cover in the eastern North Atlantic – reminiscent of the CLIMAP SST reconstruction for LGM (CLIMAP, 1981) – and hence too cold sea surface conditions compared to proxy data (Fig. S1 in the Supplement). Subsequent adjustments of the CLIMAP reconstruction (e.g. Paul and Schäfer-Neth, 2003; Torac-inta et al., 2004) suggest that the LGM sea-ice margin was located further north in the eastern North Atlantic – structurally more similar to the one obtained in the simulation with PI OHT (Fig. S1 in the Supplement). Therefore, the analyses in this study are mostly based on the simulations with PI OHT, whereas the simulations with LGM OHT are primarily used for sensitivity purposes (Sect. 4.2).

To evaluate the impact of the North American ice sheet on the Eurasian climate, we carried out six additional simulations with CAM3 specifically for this study. These simulations are identical to the PDoro simulations except that we include only the Eurasian ice sheets but keep the present-day orography elsewhere (hereafter referred to as the "EAonly" simulations). The EAonly simulations are conducted with both OHT parameterizations for all glacial time slices. The impact of the North American ice sheet on the climate is evaluated as the difference between the fullGlacial and EAonly simulations. Note that the influence of the North American ice sheet could also be calculated as the difference between equivalent "NAonly" (simulations with ice sheets in North America but present-day orography elsewhere) and the PDoro simulations. However, such ap-

CPD
11, 5203–5241, 2015

proach is less satisfactory as it would omit feedbacks from the Eurasian ice sheet, and thus most likely inhibit ice growth.

For each time slice, the orbital clock (Berger and Loutre, 1991) and greenhouse gas concentrations (Petit et al., 1999; Spahni et al., 2005) were adjusted to the nominal time of the ice-sheet reconstruction (Table 1). Other boundary conditions, e.g. vegetation, aerosols and landfraction were set to pre-industrial values in all simulations (Löfverström et al., 2014). As reference climate, we use an equilibrated present-day simulation from the same model (Hurrell et al., 2006).

2.2 Ice-sheet model

2.2.1 Model description

To simulate the evolution of the Eurasian ice sheet, we use the three-dimensional ice-sheet model SICOPOLIS (SImulation COde for POLythermal Ice Sheets, version 3.1), which treats ice as an incompressible, viscous and heat-conducting fluid (Greve, 1997). The model equations are subjected to the shallow-ice approximation, which means that only the lowest order terms are retained (Hutter, 1983). The model obeys Glen's flow law to calculate strain rates (deformation) from the applied stresses (e.g. Van der Veen, 2013), and a Weertman-type sliding to calculate the basal velocities (Weertman, 1964). Ice streams are not specifically treated. We run the model in the "cold-ice mode", i.e. temperatures above the pressure melting point are artificially reset to the pressure melting temperature. Expansion of marine ice is allowed if the bathymetry is less than 500 m (default value), otherwise instant calving is assumed. The bedrock and ice sheet are assumed to relax toward isostatic equilibrium with a timescale of 3 kyrs, and the geothermal heat flux is 55 mW m^{-2} over the entire domain.

The surface mass balance is given by the difference between accumulation and ablation. In SICOPOLIS, accumulation is equal to precipitation and the ablation is parameterized using the positive degree day (PDD) approach (Braithwaite and Olesen, 1989; Reeh, 1991). The amount of PDDs in a year is given by the integrated sum of

CPD
11, 5203–5241, 2015

positive temperatures over that year, and is evaluated using the semi-analytical solution in Calov and Greve (2005). It is assumed that the daily temperatures in a month are normally distributed about the monthly-mean temperature. The standard deviation (day-to-day variability) of the temperature is 5 °C everywhere (default). We use the default values of the degree-day constants, which relate the PDDs to actual melt rates (3 mm day^{-1} K^{-1} for snow and 12 mm day^{-1} K^{-1} for ice). The melting procedure follows Reeh (1991). The first PDDs are used to melt the annual snow fall. It is assumed that 60 % of that melt water percolates down the ice and contributes to the formation of superimposed ice. Second, the superimposed ice is melted, after which the remaining PDDs, if any, are used to melt the glacier ice.

Following Charbit et al. (2002) and Charbit et al. (2007), the surface temperature (T) and precipitation (P) over the evolving ice sheet are modified according to a fixed atmospheric lapse rate γ:

$$T(t) = T_0 + \gamma(z(t) - z_0), \quad (1)$$

$$P(t) = P_0 \exp(\gamma_s \gamma(z(t) - z_0)), \quad (2)$$

where $z(t)$ is the height of the evolving ice-sheet surface (t = time), and T_0 and P_0 are the reference temperature and precipitation on the initial ice-free topography z_0, respectively (see Eqs. 3 and 4 in Sect. 2.2.2). Hence, it is assumed that the T decreases linearly with z at the rate γ (set to value of the standard atmosphere: $\gamma = -6.5 \times 10^{-3}$ K m^{-1}), and that P decreases exponentially with the temperature change (due to elevation) times the parameter γ_s, which relates the temperature anomaly to precipitation change (set to $\gamma_s = 0.05$ K^{-1} following Charbit et al., 2002, 2007). Because the surface temperature on the ice sheet is progressively evolving in time, the relative amount of solid and liquid precipitation is parameterized; the fraction snowfall to the total precipitation is one if the monthly-mean air temperature is below −10 °C, and zero if it is greater than 7 °C. For intermediate temperatures the fraction snowfall is linearly interpolated.

CPD
11, 5203–5241, 2015

2.2.2 Experimental approach and initial climate forcing

The SICOPOLIS simulations are carried out to steady-state (at least 150 kyrs) from an ice-free initial state using the CAM3 simulations as climate forcing. The horizontal resolution is set to 80 km, and the model domain covers most of the Northern Hemisphere. The relatively coarse horizontal resolution is motivated by the fact that we are primarily interested in larger scale first-order changes of the Eurasian ice sheet (as reference, Kleman et al., 2013, used a horizontal resolution of 95 km in their ice-sheet reconstructions). The vertical resolution amounts to 81 levels in the ice and 11 levels in the bedrock.

We use the procedure described in Charbit et al. (2007) to deduce the initial fields of surface temperature T_0 and precipitation P_0 from the atmospheric model:

$$T_0 = T_{\mathrm{PD,obs}} + T_{\mathrm{paleo,CAM}} - T_{\mathrm{PD,CAM}} - \gamma(z_{\mathrm{paleo}} - z_{\mathrm{PD}}), \quad (3)$$

$$P_0 = P_{\mathrm{PD,obs}} \times (P_{\mathrm{paleo,CAM}}/P_{\mathrm{PD,CAM}}) \times \exp[-\gamma_s\gamma(z_{\mathrm{paleo}} - z_{\mathrm{PD}})]. \quad (4)$$

To account for systematic biases in the atmospheric model we first calculate anomalies of the glacial temperature ($T_{\mathrm{paleo,CAM}}$) with respect to the temperature of the present-day simulation ($T_{\mathrm{PD,CAM}}$). In doing so, we correct for the different orographies in the glacial and present-day simulations ($z_{\mathrm{paleo,CAM}}$ and $z_{\mathrm{PD,CAM}}$, respectively) using the standard lapse rate. Subsequently, the anomalies are bi-linearly interpolated to the SICOPOLIS grid and added to the observational dataset ($T_{\mathrm{PD,obs}}$), which is based on ERA-Intirim reanalysis data (Dee et al., 2011). To calculate P_0 we use the same technique as for T_0, but we use ratios instead of anomalies in order to avoid negative precipitation (Charbit et al., 2007).

CPD
11, 5203–5241, 2015

3 Results

3.1 Atmospheric response

3.1.1 Summer temperature

The annual ablation is dominated by the summer conditions; we therefore focus on the surface temperature in boreal summer (June–August: JJA). Figure 2 shows the JJA surface temperature in the ERA-Interim (Dee et al., 2011) reanalysis data (a), present-day simulation (b) and the EAonly simulations (c, e, g). To highlight areas susceptible for inception, the temperatures in Fig. 2 are projected to the present-day orography using the standard lapse rate. A summary of the average summer temperatures in the Northern Hemisphere and Eurasia is presented in Table 2.

The average Northern Hemisphere summer temperature decreases across the simulations; it drops by 3 °C between present-day and MIS5b, and by an additional 2 °C at LGM (Table 2). The progressive cooling across the glacial simulations has even larger regional variations: in Eurasia, the LGM summer temperature is about 5 °C lower than at MIS5b (Table 2). Regions with sub-freezing summer temperatures are particularly interesting for glacial inception – the average position of the zero-degree summer (surface) isotherm in indicated by the green contour in Fig. 2a, b, c, e, g. Similar to present-day (Fig. 2a, b), the zero-degree isotherm at MIS5b is mainly located in the Arctic Ocean poleward of the Eurasian continent (Fig. 2c). Owing to the cooler conditions at MIS4 and LGM, the (zonal) average location of the zero-degree isotherm is shifted approximately 6 to 7° equatorward (Table 2); the largest regional changes are found in Scandinavia and eastern Siberia, where it reaches as far south as 60° N at MIS4 and LGM (Fig. 2e, g).

Figure 2d, f, h shows the summer temperature anomalies induced by the North American ice sheet. These anomalies are calculated as the difference between the fullGlacial and EAonly simulations; a lapse rate correction has been applied to account for elevation differences. Due to an increased surface albedo and cold air advection

CPD
11, 5203–5241, 2015

by orographically forced stationary waves (Cook and Held, 1988; Roe and Lindzen, 2001; Abe-Ouchi et al., 2007; Liakka and Nilsson, 2010; Liakka, 2012; Löfverström et al., 2015), the largest cooling occurs in the vicinity of the North American ice sheet. In Eurasia, the temperature response to the North American ice sheet exhibits large regional variations. For all time slices, the North American ice sheet induces colder conditions in Europe, whereas the response in Siberia is more complicated; at MIS5b the Siberian temperature response is almost negligible (Fig. 2d), whereas there is a warming in eastern Siberia at MIS4 and LGM. The largest difference between MIS4 and LGM responses is found in central Siberia, which is cooler at MIS4 (Fig. 2f) and warmer at LGM (Fig. 2h).

3.1.2 Annual precipitation

The large-scale features of the annual precipitation in the EAonly simulations are reminiscent of the modern climate, although the global precipitation rates are somewhat reduced in the glacial simulations (Fig. 3a, b, c, e, g). The largest precipitation rates in Eurasia are found in northwestern Europe where the cyclones from the Atlantic storm-track make landfall.

As for the temperature, the largest precipitation response to the North American ice sheet is found locally, with generally increased precipitation on the windward (westerly) slopes of the ice sheet and reduced precipitation over the leeward (easterly) slopes (Fig. 3d, f, h). In Eurasia, the North American ice sheet has a relatively small impact on the precipitation at MIS5b and MIS4 (Fig. 3d, f), but yields a significantly reduced precipitation in northwestern Europe at LGM (Fig. 3h). As discussed in Löfverström et al. (2014), the reduced precipitation rates at LGM is associated with a zonalisation of the midlatitude Atlantic jet stream resulting from flow-topography interactions with the continent-wide North American ice sheet at LGM (Li and Battisti, 2008; Ullman et al., 2014; Merz et al., 2015). Löfverström et al. (2014) found that this effect is not present for the smaller pre-LGM ice sheets (MIS5b and MIS4), as their location and

CPD
11, 5203–5241, 2015

spatial extent allow the mean-flow to largely circumvent the topography, thus rendering the tilt of the Atlantic jet – and stormtrack – largely similar to the present-day.

3.1.3 Summer stationary waves

To gain some insight into the temperature response in Fig. 2, we examine the stationary Rossby waves in the different climate states. Stationary waves, defined as zonal asymmetries in the climatological fields, are the result of large scale orography and diabatic heating (e.g. Hoskins and Karoly, 1981; Held et al., 2002; Held, 1983; Kaspi and Schneider, 2011). Ice sheets constitute both orographic and diabatic forcing of stationary waves. Therefore, ice sheets expanding into the westerly mean flow can potentially influence the global stationary wave field (e.g. Cook and Held, 1988; Roe and Lindzen, 2001; Löfverström et al., 2014).

The lower troposphere (700 hPa) geopotential height anomalies from the EAonly simulations are shown in Fig. 4c, e, g. The stationary wave response is qualitatively similar in all glacial time slices; similar to the modern climate (Fig. 4a, b), the summer stationary wave field is characterized by anticyclonic circulation (ridges) over the subtropical Pacific and Atlantic ocean basins, and cyclonic circulation (troughs) over Asia and northeastern Canada (Fig. 4c, e, g). In addition, the ridge over the Atlantic Ocean extends over Europe and covers most of the ice sheet area, suggesting that the local ridge is excited by the ice sheet. As noted by Löfverström et al. (2014), this indicates that the ice sheet's diabatic cooling is dominating the stationary wave response.

The 700 hPa height responses to the North American ice sheets are shown as shading in Fig. 4d, f, h. As expected from theory, the stationary wave amplitudes increases with the size (spatial extent and height) of the North American ice sheet (Cook and Held, 1992; Ringler and Cook, 1997; Liakka and Nilsson, 2010; Liakka et al., 2011; Löfverström et al., 2014). Besides the amplitude, the stationary wave response to the North American ice sheet is qualitatively similar in all time slices. The local response is a ridge over the northwestern parts of the North American ice sheet and a trough in the southeast. This particular response is a robust feature across models using non-

CPD
11, 5203–5241, 2015

linear stationary wave dynamics (Ringler and Cook, 1997, 1999; Liakka et al., 2011). The remote downstream response consists of two wavetrains: (i) a subtropical wavetrain with a northwest-southeast orientation, and (ii) a low wavenumber polar wavetrain with a more zonal orientation. The polar wavetrain is characterized by a trough over Europe/western Asia and a ridge over Siberia.

The contours in Fig. 4d, f, h depict the height anomalies at 300 hPa. Note that the anomalies at this level have essentially the same location as at 700 hPa, indicating that the climatological response to the North American ice sheet is largely equivalent barotropic.

In the summer season, high-latitude height anomalies are typically well correlated with anomalies of the surface temperature. Ridges are associated with reduced cloudiness and increased downwelling shortwave radiation, which leads to a surface warming, whereas troughs typically yield increased cloudiness and thus lower surface temperatures. This is also seen here (cf. Figs. 2d, f, h and 4d, f, h): the ridge over eastern Siberia and Alaska is associated with a surface warming, and the trough in Europe with colder conditions. Note that the magnitude of these temperature anomalies, in particular the Siberian warm anomaly, is not only controlled by the height anomalies, but also by albedo feedbacks due to changes in the snow cover (see Fig. S2).

3.2 Ice-sheet evolution

In this section we examine how the altered climate conditions – induced by the North American ice sheet – influence the spatial equilibrium extent of the Eurasian ice sheet. To evaluate our results, we compare the simulated extents of the Eurasian ice sheet with the geologically-constrained reconstructions from Kleman et al. (2013). Note that we only compare the geographical distribution of ice (i.e. ice area), but not the ice thickness or ice volume. The reason is that the ice thickness in the Kleman et al. (2013) reconstructions is a model dependent feature, whereas the spatial extents are constrained by geological evidence.

CPD
11, 5203–5241, 2015

Figure 5 shows the simulated equilibrium ice thickness when using the atmospheric simulations summarized in Figs. 2 and 3 as climate forcing. Apart from some ice caps in the Scandinavian mountains, Eurasia remains virtually ice free at MIS5b (Fig. 5a, b). This is consistent with a negative surface mass balance over essentially the entire domain (Fig. S3). A comprehensive discussion on the potential shortcomings in the MIS5b simulations follows in Sect. 4.3.

At MIS4 and LGM, atmospheric circulation changes induced by the North American ice sheet serves to increase the total ice area in Eurasia by about 80 and 30 %, respectively (Fig. 5). This increase is mediated by an expansion of ice in Europe and a reduced ice extent in eastern Siberia; apart from somewhat too much ice in the Kara-sea region in the LGM simulation, the outlines of the simulated MIS4 and LGM ice sheets in Eurasia are in good agreement with the reconstructions from Svendsen et al. (2004) and Kleman et al. (2013) (Fig. 5d, f). In the absence of ice in North America, the MIS4 and LGM ice sheets are fairly zonally distributed along the Arctic coast (Fig. 5c, e). Hence, our simulations suggest that the North American ice sheet induces a westward migration of the Eurasian ice sheet; as a result the evolution of the Eurasian ice sheet between MIS4 and LGM was to a large extent controlled by the growth of the North American ice sheet.

The ice sheet's westward migration is elucidated in Fig. 6, which shows the longitude of the center of mass (λ_c). In the reconstructions from Kleman et al. (2013), λ_c decreases from 49° E at MIS5b to 44° E and 27° E at MIS4 and LGM, respectively (black bars in Fig. 6). Note that the westward migration between MIS4 and LGM is captured only if the North American ice sheet is present (white bars in Fig. 6), otherwise λ_c remains large (~ 55–60° E) for both stages (grey bays in Fig. 6).

4 Discussion

We have examined how the North American ice sheet (constrained by geological data) influences the extent of the Eurasian ice sheet in the MIS5b, MIS4 and LGM climate

CPD
11, 5203–5241, 2015

states. We found that the MIS4 and LGM ice sheets in North America yield a westward migration of the Eurasian ice sheet (Fig. 6), characterized by more ice in Europe and less ice in Siberia (Fig. 5). In the presence of the North American ice sheet, the spatial distributions of the simulated MIS4 and LGM ice sheets in Eurasia are in good agreement with contemporary ice-sheet reconstructions (Fig. 5; Svendsen et al., 2004; Kleman et al., 2013); this suggests that the growth of the North American ice sheet between MIS4 and LGM may have been vital for the westward migration of the Eurasian ice sheet during this time.

The discussion is divided into three parts. First, in Sect. 4.1 we analyse the stationary wave response to the North American ice sheet – and the associated westward migration of Eurasian ice sheet – from a theoretical perspective by employing linear theory. Second, because the simulated ice sheets presented thus far have been based on atmospheric simulations with a constant (pre-industrial) OHT, we investigate the sensitivity of our results to the OHT in Sect. 4.2. This exercise is particularly relevant because of the large uncertainty associated with changes of the Atlantic Meridional Overturning Circulation (AMOC) in glacial climates (Weber et al., 2007). Finally, in Sect. 4.3, potential reasons for the lack of ice growth in our MIS5b experiment are discussed. Since the simulated MIS4 and LGM ice extents – that are in agreement with the data-based reconstructions – were obtained using essentially the default parameters in SICOPOLIS, we will not explore the entire parameter space of the model to induce ice-sheet inception for MIS5b. Instead, the discussion focuses on potential issues with the experimental approach.

4.1 Westward migration of the Eurasian ice sheet

The westward migration of the Eurasian ice sheet in the MIS4 and LGM simulations (Figs. 5 and 6) is associated with changes in the summer stationary wave field. It is found that the North American ice sheet yields a cooling (less ablation) in Europe and a warming (more ablation) in northeastern Siberia (Fig. 2f, h). These temperature anomalies are associated with an equivalent barotropic cyclonic/anticyclonic structure

CPD
11, 5203–5241, 2015

in the target regions; this is particularly true for the low wavenumber anomalies at high latitudes (Fig. 4f, h). For example, the more westward location of the Siberian warm anomaly at the LGM than at MIS4 is associated with a more westward extent of the Siberian ridge.

The height anomalies in Fig. 4d, f, h result from (typically nonlinear) interactions between the atmospheric flow and the thermal and orographic forcing of the North American ice sheet. Due to the complexity of the atmospheric model, it is useful to resort to simpler linear models to gain a conceptual understanding of the stationary wave field. Linear models have been shown to qualitatively capture the large-scale features of the stationary waves in the present-day atmosphere (Charney and Eliassen, 1949; Held, 1983; Held et al., 2002). However, many features omitted in linear models, such as zonal variations in the background state and (nonlinear) wave-wave interactions can significantly alter the stationary wave response (e.g. Cook and Held, 1992; Hoskins and Ambrizzi, 1993; Ringler and Cook, 1997). Therefore, results from linear models should only be considered as a qualitative first-order estimate of the total wave response. The equivalent barotropic structure in Fig. 4d, f, h suggests that the stationary wave response to the North American ice sheet is dominated by orographic rather than thermal forcing; the latter has been shown to yield stationary waves with a more baroclinic structure (height anomalies tilt westward with altitude Hoskins and Karoly, 1981; Ting, 1994; Ringler and Cook, 1999). Therefore, we use the linear barotropic model in spherical geometry with orographic forcing to analyse the wave response. This is the simplest model that can be used to study meridional dispersion of stationary waves (Held, 1983). In particular, the linear Rossby wave ray tracing theory provided in Hoskins and Karoly (1981) is useful for analysing the disposition of stationary wavetrains.

In models linearized about a zonal mean basic state, the horizontal scale of the stationary waves is given by the "stationary wavenumber" K_s, which is a function of the

CPD
11, 5203–5241, 2015

atmospheric background state. In the barotropic model, K_s is given by (Held, 1983):

$$K_s^2 = k^2 + l^2 = \cos^2\phi \left(\frac{\beta + a^{-1}\partial[\zeta]/\partial\phi}{[u]} \right), \quad (5)$$

where β and $a^{-1}\partial[\zeta]/\partial\phi$ are the meridional gradients of planetary and (zonal mean) relative vorticity, $[u]$ is the zonal mean background flow, ϕ the latitude and k and l denote zonal and meridional wavenumbers, respectively. In the present-day atmosphere (Hoskins and Karoly, 1981; Held, 1983) as well as in our simulations (Fig. 7), K_s is a monotonically decreasing with latitude (as β and $cos(\phi) \rightarrow 0$ towards the pole). This implies that stationary waves at high latitudes typically have lower zonal wavenumbers than those propagating at lower latitudes. Hence, the low wavenumber response at high latitudes in Fig. 4d, f, h ($> 60^{\circ}$N) is essentially a result of the small K_s due to the spherical geometry of the planet.

Following Hoskins and Karoly (1981), the propagation direction of stationary waves is given by the direction of the local group velocity: $c_g = (c_{gx}i, c_{gy}j)$. Because c_{gy} is identical to c_{gx} except for a factor l instead of a k[1] (Hoskins and Karoly, 1981; Vallis, 2006), the inclination (α) of the ray path (propagation direction) is given by:

$$\tan\alpha = \frac{c_{gy}}{c_{gx}} = \frac{l}{k}. \quad (6)$$

Here, k is constant along a ray; hence as K_s decreases with latitude (Fig. 7), $|l|$ must decrease to satisfy Eq. 5. This implies that waves at high latitudes propagate along more zonal paths than waves at lower latitudes (Eq. 6); this is seen also in Fig. 4d, f,

[1]For stationary waves, $c_{gx} = 2\beta k^2/(k^2 + l^2)^2$ and $c_{gy} = 2\beta kl/(k^2 + l^2)^2$. Hence, $c_{gx} > 0$, which implies that the wave energy always propagates eastward. c_{gy}, on the other hand, depends on the sign of l, which corresponds to poleward (positive l) and equatorward (negative l) propagation.

CPD
11, 5203–5241, 2015

h, where the polar wavetrain is more zonally oriented than the subtropical wavetrain. Hence, despite the high complexity of the atmospheric circulation model used here, the key features (wavenumber and orientation) of the polar wavetrain in Fig. 4d, f, h – that are associated with the westward migration of the Eurasian ice sheet – are consistent with linear barotropic theory. This suggests that simplified atmospheric circulation models, which capture the fundamental dynamics, can be used to study teleconnections between the North American and Eurasian ice sheets.

4.2 Sensitivity to OHT

One of the main drawbacks with the model setup used in this study is that it does not have an interactive dynamic ocean model that responds to changes in the atmospheric circulation. For the Eurasian climate, changes in the Atlantic meridional overturning circulation (AMOC) are particularly important as it transports warm surface water poleward and thereby influences the mean position of the sea-ice margin in the North Atlantic (Bitz et al., 2005). The strength of AMOC during glacial times is highly model dependent; for the LGM some of the coupled atmosphere–ocean models in the Paleomodeling Intercomparison Project (PMIP) yield a strengthening of the AMOC compared to present-day whereas others yield a weakening (Otto-Bliesner et al., 2007; Weber et al., 2007). In addition, results diverge within the same model family; CCSM3 exhibits a general weakening of the AMOC for LGM, ultimately ending up with the "CLIMAP-like" sea-ice cover in Brandefelt and Otto-Bliesner (2009) (LGM OHT in Supplement Fig. S1), whereas the more recent model CCSM4 yields a slightly increased AMOC (Brady et al., 2013).

Owing to the large uncertainty of the AMOC response during glacial times, we perform sensitivity simulations of the equilibrium ice thickness using the atmospheric simulations with the OHT derived from Brandefelt and Otto-Bliesner (2009) (LGM OHT) as climate forcing. The results are summarized in Fig. 8. Due to the colder conditions in the simulations with LGM OHT, the Eurasian ice sheet expands equatorward compared to when using PI OHT (cf. Figs. 8 and 5). Notably, despite the colder conditions

CPD
11, 5203–5241, 2015

in the North Atlantic, the model fails to simulate a sufficiently large ice sheet for MIS5b (Fig. 8a, b). Compared to the PI OHT simulations, the MIS4 and LGM ice sheets are significantly larger in the LGM OHT simulations (Fig. 8c–f). The North American ice sheet yields a westward migration of the Eurasian ice sheet also in the LGM OHT simulations (λ_c is reduced by 6° for MIS4 and by 11° for LGM; not shown); however, it is not as pronounced as in the PI OHT simulations (Fig. 6). Because the climate response to the North American ice sheet is qualitatively similar in the LGM OHT (Figs. S4, S5 and S6) and the PI OHT simulations (Figs. 2, 3 and 4), the reduced westward migration in the LGM OHT simulations is most likely attributed to a colder climate; in the PDD model, cold background conditions (temperatures below freezing) reduces the effect of temperature anomalies on the ablation.

4.3 What prevents ice-sheet growth at MIS5b?

The vexing issue of this study is that we fail to simulate a MIS5b ice sheet of comparable size to the data-based reconstructions (Fig. 5) – even when using the colder LGM OHT climate conditions (Fig. 8). The lack of ice growth at MIS5b is associated with a negative surface mass balance across the entire Eurasian continent (Fig. S3) due to relatively high summer temperatures (Fig. 2 and Table 2). The relatively warm conditions at MIS5b compared to MIS4 and LGM are attributed to a higher insolation and greenhouse gases concentrations (Table 1). It is possible that allowing for certain feedbacks, such as vegetation changes (Colleoni et al., 2009; Liakka et al., 2014), would cool the summer climate and thus support ice inception at MIS5b. However, because the MIS4 and LGM extents of the Eurasian ice sheets are in good agreement with the reconstructions when omitting these feedbacks, it seems unlikely that systematic biases in the climate forcing is the primary cause for the lack of ice growth at MIS5b.

Possibly, missing processes in the ice-sheet model inhibit the early development of ice sheets. For example, SICOPOLIS does not treat ice streams so there is no use of the shallow-shelf approximation (SSA; Macayeal, 1989); this considerably reduces the basal velocities (Macayeal, 1989). Under relatively warm conditions (such

CPD
11, 5203–5241, 2015

as MIS5b), the use of SSA could trigger higher velocities in some areas and thereby cause a faster expansion of the ice sheet. The faster ice expansion, along with the ensuing temperature-elevation feedback, could in some cases compensate for a negative surface mass balance and thus support ice-sheet inception.

However, the most obvious caveats are associated with the setup of our experiments. All the ice-sheet model simulations conducted here were integrated to equilibrium starting from ice-free (bare ground) conditions. The good agreement between the simulated MIS4 and LGM extents and the proxy suggests that these ice sheets were essentially in equilibrium with the prevailing climate; this is, however, not necessarily true for MIS5b. Instead, it is plausible that the MIS5b ice sheet is a remnant of preceding ice-sheet configurations and climate conditions. In this context it is interesting to note that the Eurasian ice sheet reached a size comparable to MIS5b already at ∼ 105 kyrs BP, subsequent to a relative minimum in the high-latitude boreal summer insolation (Kleman et al., 2013; Löfverström et al., 2014).

In order to test the effect of the ice-sheet and climate history on the extent of the MIS5b ice sheet, we conduct two sensitivity experiments in SICOPOLIS. In the first experiment, we use the Kleman et al. (2013) reconstruction in Eurasia (Fig. 1a) instead of an ice-free state as initial condition. Initializing the model with a pre-existing ice sheet yields lower initial temperatures on the ice sheet (due to the atmospheric lapse rate) than with bare ground. In the simulations initialized with the Kleman et al. (2013) reconstruction, the ice extent increases slightly in the Barents sea region compared to the simulations initiated from an ice-free state (Fig. 9a, b). Aside from that, however, Eurasia remains predominately ice-free also when using the reconstructed ice sheet as initial condition.

In the second experiment we test the sensitivity of the extent of the MIS5b ice sheet to the colder climate history. Because we do not have access to any atmospheric simulations of a colder stages prior to MIS5b, we use a crude approach by imposing a cooling of the JJA temperature artificially in SICOPOLIS. To estimate the magnitude of the cooling, we employ the parameterization of the surface temperature to changing inso-

CPD
11, 5203–5241, 2015

lation in Abe-Ouchi et al. (2007, 2013); based on sensitivity experiments with a coupled atmosphere–ocean model, they obtained a linear relationship between changes of the high-latitude temperature ($\Delta T_{\mathrm{insol}}$) and insolation ($\Delta Q$): $\Delta T_{\mathrm{insol}} = 3.25 \times \Delta Q/40$. The insolation at the youngest minimum preceding MIS5b (at ~ 95 kyrs BP) was about 40 $\mathrm{W\,m^{-2}}$ lower than at MIS5b (Berger and Loutre, 1991); this yields $\Delta T_{\mathrm{insol}} \approx -3^{\circ}\mathrm{C}$. Using the colder "minimum insolation" conditions, the extent of the Eurasian ice sheet agrees well with the MIS5b reconstruction in Scandinavia and the Barents sea region (Fig. 9c, d) – in particular when the North American ice sheet is included (Fig. 9d) – whereas the Kara sea region continually remains ice free. Hence, in contrast to MIS4 and LGM, our first-order sensitivity analysis suggests that the MIS5b extent of the Eurasian ice sheet is predominately a result of preceding colder stages rather than the prevailing climate.

5 Conclusions

We have examined the impact of the geologically-constrained MIS5b, MIS4 and LGM ice sheets in North America on the spatial extent of the Eurasian ice sheet. The conclusions are summarized as follows:

- The North American ice sheet yields a cooler summer temperatures in Europe and warmer temperatures in northeastern Siberia in all time slices. The amplitude of these anomalies and the westward extent of the Siberian warming increase with the size of the North American ice sheet (Fig. 2).
- The temperature anomalies are associated with a equivalent barotropic cyclone and anticyclone in Europe and Siberia, respectively (Fig. 4). The structure of the circulation anomalies is qualitatively consistent with linear barotropic stationary wave theory.
- Owing to its impact on the Eurasian summer temperatures, the North American ice sheet controls the westward migration of the Eurasian ice sheet; in the

CPD
11, 5203–5241, 2015

presence of the North American ice sheet, the spatial extents of the simulated Eurasian ice sheets at MIS4 and LGM are consistent with contemporary ice-sheet reconstructions (Svendsen et al., 2004; Kleman et al., 2013). However, if the North American ice sheet is omitted, the Eurasian ice sheet becomes more zonally distributed with a more eastward located center of mass (Figs. 5, 6).

– Although the spatial extents of the MIS4 and LGM ice sheets are well captured by SICOPOLIS, Eurasia remains essentially ice free for MIS5b. Unlike MIS4 and LGM, first-order sensitivity analysis reveals that the MIS5b ice sheet was not in equilibrium with the prevailing climate, but most likely a result of preceding colder climate conditions.

– Our study suggests that the westward migration of the Eurasian ice sheet between MIS4 and LGM was induced by the expansion of the North American ice sheet. Furthermore, our results is consistent with the notion that the east-heavy Eurasian ice sheet at the late Saalian Maximum (~ 140 kyrs BP) was accompanied by a relatively small ice sheet in North America (Svendsen et al., 2004; Colleoni et al., 2014).

The Supplement related to this article is available online at doi:10.5194/cpd-11-5203-2015-supplement.

Acknowledgements. We are grateful to Johan Kleman for providing the ice-sheet reconstructions. We acknowledge support from the research funding programme "LOEWE-Landesoffensive zur Entwicklung Wissenschaftlich-ökonomischer Exzellenz" of Hesse's Ministry of Higher Education. The LOEWE initiative also provided financial support for the simulations, which were carried out at the LOEWE Frankfurt Centre for Scientific Computing (LOEWE-CSC).

CPD
11, 5203–5241, 2015

References

Abe-Ouchi, A., Segawa, T., and Saito, F.: Climatic Conditions for modelling the Northern Hemisphere ice sheets throughout the ice age cycle, Clim. Past, 3, 423–438, doi:10.5194/cp-3-423-2007, 2007. 5213, 5223

Abe-Ouchi, A., Saito, F., Kawamura, K., Raymo, M. E., Okuno, J., Takahashi, K., and Blatter, H.: Insolation-driven 100,000-year glacial cycles and hysteresis of ice-sheet volume, Nature, 500, 190–193, 2013. 5223

Beghin, P., Charbit, S., Dumas, C., Kageyama, M., Roche, D. M., and Ritz, C.: Interdependence of the growth of the Northern Hemisphere ice sheets during the last glaciation: the role of atmospheric circulation, Clim. Past, 10, 345–358, doi:10.5194/cp-10-345-2014, 2014. 5205, 5207

Berger, A. and Loutre, M.-F.: Insolation values for the climate of the last 10 million years, Quaternary Sci. Rev., 10, 297–317, 1991. 5205, 5209, 5223, 5231

Bitz, C., Holland, M., Hunke, E., and Moritz, R.: Maintenance of the sea-ice edge, J. Climate, 18, 2903–2921, 2005. 5220

Bonelli, S., Charbit, S., Kageyama, M., Woillez, M.-N., Ramstein, G., Dumas, C., and Quiquet, A.: Investigating the evolution of major Northern Hemisphere ice sheets during the last glacial-interglacial cycle, Clim. Past Discuss., 5, 1013–1053, doi:10.5194/cpd-5-1013-2009, 2009. 5205

Bradwell, T., Stoker, M. S., Golledge, N. R., Wilson, C. K., Merritt, J. W., Long, D., Everest, J. D., Hestvik, O. B., Stevenson, A. G., Hubbard, A. L., et al.: The northern sector of the last British Ice Sheet: maximum extent and demise, Earth-Sci. Rev., 88, 207–226, 2008. 5205

Brady, E. C., Otto-Bliesner, B. L., Kay, J. E., and Rosenbloom, N.: Sensitivity to glacial forcing in the CCSM4, J. Climate, 26, 1901–1925, 2013. 5220

Braithwaite, R. J. and Olesen, O. B.: Calculation of glacier ablation from air temperature, West Greenland, in: Glacier Fluctuation and Climate Change, edited by: Oerlemans, J., Kluwer, Dordrecht, 219–233, 1989. 5209

Brandefelt, J. and Otto-Bliesner, B. L.: Equilibration and variability in a Last Glacial Maximum climate simulation with CCSM3, Geophys. Res. Lett., 36, L19712, doi:10.1029/2009GL040364, 2009. 5208, 5220

Calov, R. and Greve, R.: A semi-analytical solution for the positive degree-day model with stochastic temperature variations, J. Glaciol., 51, 173–175, 2005. 5210

CPD
11, 5203–5241, 2015

Charbit, S., Ritz, C., and Ramstein, G.: Simulations of Northern Hemisphere ice-sheet retreat:. sensitivity to physical mechanisms involved during the Last Deglaciation, Quaternary Sci. Rev., 21, 243–265, doi:10.1016/S0277-3791(01)00093-2, 2002. 5210

Charbit, S., Ritz, C., Philippon, G., Peyaud, V., and Kageyama, M.: Numerical reconstructions of the Northern Hemisphere ice sheets through the last glacial-interglacial cycle, Clim. Past, 3, 15–37, doi:10.5194/cp-3-15-2007, 2007. 5205, 5210, 5211

Charney, J. G. and Eliassen, A.: A numerical method for predicting the perturbations of the middle latitude westerlies, Tellus A, 1, 38–55, 1949. 5218

Clark, P. U., Clague, J. J., Curry, B. B., Dreimanis, A., Hicock, S. R., Miller, G. H., Berger, G. W., Eyles, N., Lamothe, M., Miller, B. B., Mott, R. J., Oldale, R. N., Stea, R. R., Szabo, J. P., Thorleifson, L. H., and Vincent, J.-S.: Initiation and development of the Laurentide and Cordilleran ice sheets following the last interglaciation, Quaternary Sci. Rev., 12, 79–114, 1993. 5205

CLIMAP: Seasonal reconstructions of the Earth's surface at the last glacial maximum, Technical Report MC-36, Geological Society of America, Boulder, CO, 1981. 5208

Colleoni, F., Krinner, G., and Jakobsson, M.: Sensitivity of the Late Saalian (140 kyrs BP) and LGM (21 kyrs BP) Eurasian ice sheet surface mass balance to vegetation feedbacks, Geophys. Res. Lett., 36, 8, doi:10.1029/2009GL037200, 2009. 5221

Colleoni, F., Wekerle, C., and Masina, S.: Long-term safety of a planned geological repository for spent nuclear fuel in Forsmark – estimate of maximum ice sheet thicknesses, Technical Report SKB TR-14-21, SKB, 2014. 5224

Collins, W. D., Rasch, P. J., Boville, B. A., Hack, J. J., McCaa, J. R., Williamson, D. L., Briegleb, B. P., Bitz, C. M., Lin, S.-J., and Zhang, M.: The formulation and atmospheric simulation of the Community Atmosphere Model: CAM3, J. Climate, 19, 2144–2161, 2006. 5207

Cook, K. H. and Held, I. M.: Stationary waves of the ice age climate, J. Climate, 1, 807–819, 1988. 5213, 5214

Cook, K. H. and Held, I. M.: The stationary response to large-scale orography in a general circulation model and a linear model, J. Atmos. Sci., 49, 525–539, 1992. 5214, 5218

Dee, D. P., Uppala, S. M., Simmons, A. J., Berrisford, P., Poli, P., Kobayashi, S., Andrae, U., Balmaseda, M. A., Balsamo, G., Bauer, P., Bechtold, P., Beljaars, A. C. M., van de Berg, L., Bidlot, J., Bormann, N., Delsol, C., Dragani, R., Fuentes, M., Geer, A. J., Haimberger, L., Healy, S. B., Hersbach, H., Hólm, E. V., Isaksen, L., Kållberg, P., Köhler, M., Matricardi, M., McNally, A. P., Monge-Sanz, B. M., Morcrette, J.-J., Park, B.-K., Peubey, C., de Rosnay, P.,

CPD
11, 5203–5241, 2015

Tavolato, C., Thépaut, J.-N., and Vitart, F.: The ERA-Interim reanalysis: configuration and performance of the data assimilation system, Q. J. Roy. Meteor. Soc., 137, 553–597, 2011. 5211, 5212, 5234, 5235

Greve, R.: Application of a polythermal three-dimensional ice sheet model to the Greenland Ice Sheet: response to steady-state and transient climate scenarios, J. Clim., 10, 901–918, 1997. 5209

Held, I. M.: Stationary and quasi-stationary eddies in the extratropical troposphere: theory, in: Large-Scale Dynamical Processes in the Atmosphere, edited by: Hoskins, B. J. and Pearce, R. P., Academic Press, London, New York, 127–168, 1983. 5214, 5218, 5219

Held, I. M., Ting, M., and Wang, H.: Northern winter stationary waves: theory and modeling, J. Climate, 15, 2125–2144, 2002. 5214, 5218

Hoskins, B. J. and Ambrizzi, T.: Rossby wave propagation on a realistic longitudinally varying flow, J. Atmos. Sci., 50, 1661–1671, 1993. 5218

Hoskins, B. J. and Karoly, D. J.: The steady linear response of a spherical atmosphere to thermal and orographic forcing, J. Atmos. Sci., 38, 1179–1196, 1981. 5214, 5218, 5219

Hurrell, J. W., Hack, J. J., Phillips, A. S., Caron, J., and Yin, J.: The dynamical simulation of the Community Atmosphere Model version 3 (CAM3), J. Climate, 19, 2162–2183, 2006. 5209

Hutter, K.: Theoretical Glaciology: Material Science of Ice and the Mechanics of Glaciers and Ice Sheets, Reidel, Dordrecht, 1983. 5209

Kageyama, M., Braconnot, P., Bopp, L., Caubel, A., Foujols, M.-A., Guilyardi, E., Khodri, M., Lloyd, J., Lombard, F., Mariotti, V., Marti, O., Roy, T., and Woillez, M.-N.: Mid-Holocene and Last Glacial Maximum climate simulations with the IPSL model – Part I: Comparing IPSL_CM5A to IPSL_CM4, Clim. Dynam., 40, 2447–2468, 2013. 5206

Kaspi, Y. and Schneider, T.: Winter cold of eastern continental boundaries induced by warm ocean waters, Nature, 471, 621–624, doi:10.1038/nature09924, 2011. 5214

Kleman, J., Jansson, K., De Angelis, H., Stroeven, A. P., Hättestrand, C., Alm, G., and Glasser, N.: North American ice sheet build-up during the last glacial cycle, 115–21 kyr, Quaternary Sci. Rev., 29, 2036–2051, 2010. 5205

Kleman, J., Fastook, J., Ebert, K., Nilsson, J., and Caballero, R.: Pre-LGM Northern Hemisphere ice sheet topography, Clim. Past, 9, 2365–2378, doi:10.5194/cp-9-2365-2013, 2013. 5205, 5206, 5208, 5211, 5215, 5216, 5217, 5222, 5224, 5233, 5234, 5235, 5237, 5238, 5241

Li, C. and Battisti, D.: Reduced atlantic storminess during last glacial maximum: evidence from a coupled climate model, J. Climate, 21, 3561–3579, 2008. 5206, 5207, 5213

CPD
11, 5203–5241, 2015

Liakka, J.: Interactions between topographically and thermally forced stationary waves: implications for ice-sheet evolution, Tellus A, 64, 11088, doi:10.3402/tellusa.v64i0.11088, 2012. 5213
Liakka, J. and Nilsson, J.: The impact of topographically forced stationary waves on local ice-sheet climate, J. Glaciol., 56, 534–544, 2010. 5206, 5213, 5214
Liakka, J., Nilsson, J., and Löfverström, M.: Interactions between stationary waves and ice sheets: linear versus nonlinear atmospheric response, Clim. Dynam., 38, 1249–1262, 2011. 5206, 5214, 5215
Liakka, J., Colleoni, F., Ahrens, B., and Hickler, T.: The impact of climate-vegetation interactions on the onset of the Antarctic ice sheet, Geophys. Res. Lett., 41, 1269–1276, 2014. 5221
Löfverström, M., Caballero, R., Nilsson, J., and Kleman, J.: Evolution of the large-scale atmospheric circulation in response to changing ice sheets over the last glacial cycle, Clim. Past, 10, 1453–1471, doi:10.5194/cp-10-1453-2014, 2014. 5206, 5207, 5209, 5213, 5214, 5222
Löfverström, M., Liakka, J., and Kleman, J.: The North American Cordillera – an impediment to growing the continent-wide Laurentide Ice Sheet, J. Climate, online first, doi:10.1175/JCLI-D-15-0044.1, 2015. 5206, 5213
Macayeal, D. R.: Large-scale ice flow over a viscous basal sediment – theory and application to ice stream B, Antarctica, J. Geophys. Res., 94, 4071–4087, 1989. 5221
Marshall, S. J., Tarasov, L., Clarke, G. K., and Peltier, W. R.: Glaciological reconstruction of the Laurentide Ice Sheet: physical processes and modelling challenges, Can. J. Earth Sci., 37, 769–793, 2000. 5205
Merz, N., Raible, C. C., and Woollings, T.: North Atlantic eddy-driven jet in interglacial and glacial winter climates, J. Climate, 28, 3977–3997, 2015. 5206, 5213
Oleson,K. W., Dai, Y., Bonan, G., Bosilovich, M., Dickinson, R., Dirmeyer, P., Hoffman, F., Houser, P., Levis, S., Niu, G.-Y., Thornton, P., Vertenstein, M., Yang, Z.-L., and Zeng, X.: Technical Description of the Community Land Model (CLM), NCAR Tech. Note NCAR/TN-461+STR, Natl. Cent. for Atmos. Res., Boulder, CO, 2004. 5207
Otto-Bliesner, B., Hewitt, C., Marchitto, T., Brady, E., Abe-Ouchi, A., Crucifix, M., Murakami, S., and Weber, S.: Last Glacial Maximum ocean thermohaline circulation: PMIP2 model intercomparisons and data constraints, Geophys. Res. Lett., 34, L12706, doi:10.1029/2007GL029475, 2007. 5220
Paul, A. and Schäfer-Neth, C.: Modeling the water masses of the Atlantic Ocean at the Last Glacial Maximum, Paleoceanography, 18, 1058, doi:10.1029/2002PA000783, 2003. 5208

CPD
11, 5203–5241, 2015

Peltier, W. and Fairbanks, R. G.: Global glacial ice volume and Last Glacial Maximum duration from an extended Barbados sea level record, Quaternary Sci. Rev., 25, 3322–3337, 2006. 5205

Petit, J. R., Jouzel, J., Raynaud, D., Barkov, N. I., Barnola, J.-M., Basile, I., Bender, M., Chappellaz, J., Davis, M., Delaygue, G., Delmotte, M., Kotlyakov, V. M., Legrand, M., Lipenkov, V. Y., Lorius, C., Pépin, L., Ritz, C., Saltzman, E., and Stievenard, M.: Climate and atmospheric history of the past 420,000 years from the Vostok ice core, Antarctica, Nature, 399, 429–436, doi:10.1038/20859, 1999. 5209, 5231

Reeh, N.: Parameterization of melt rate and surface temperature on the Greenland ice sheet, Polarforschung, 59, 113–128, 1991. 5209, 5210

Ringler, T. D. and Cook, K. H.: Factors controlling nonlinearity in mechanically forced stationary waves over orography, J. Atmos. Sci., 54, 2612–2629, 1997. 5214, 5215, 5218

Ringler, T. D. and Cook, K. H.: Understanding the seasonality of orographically forced stationary waves: Interaction between mechanical and thermal forcing, J. Atmos. Sci., 56, 1154–1174, 1999. 5215, 5218

Roe, G. H.: Orographic precipitation, Annu. Rev. Earth Planet. Sci., 33, 645–671, 2005. 5206

Roe, G. H. and Lindzen, R. S.: The mutual interaction between continental-scale ice sheets and atmospheric stationary waves, J. Climate, 14, 1450–1465, doi:10.1175/1520-0442(2001)014<1450:TMIBCS>2.0.CO;2, 2001. 5206, 5213, 5214

Sanberg, J. and Oerlemans, J.: Modelling of Pleistocene European ice sheets: the effect of upslope precipitation, Geol. Mijnbouw, 62, 267–273, 1983. 5206

Spahni, R., Chappellaz, J., Stocker, T. F., Loulergue, L., Hausammann, G., Kawamura, K., Flückiger, J., Schwander, J., Raynaud, D., Masson-Delmotte, V., and Jouzel, J.: Atmospheric methane and nitrous oxide of the Late Pleistocene from Antarctic ice cores, Science, 310, 1317–1321, doi:10.1126/science.1120132, 2005. 5209, 5231

Stokes, C. R., Tarasov, L., and Dyke, A. S.: Dynamics of the North American Ice Sheet Complex during its inception and build-up to the Last Glacial Maximum, Quaternary Sci. Rev., 50, 86–104, 2012. 5205

Svendsen, J. I., Alexanderson, H., Astakhov, V. I., Demidov, I., Dowdeswell, J. A., Funder, S., Gataullin, V., Henriksen, M., Hjort, C., Houmark-Nielsen, M., et al.: Late Quaternary ice sheet history of northern Eurasia, Quaternary Sci. Rev., 23, 1229–1271, 2004. 5205, 5216, 5217, 5224

CPD
11, 5203–5241, 2015

Ting, M.: Maintenance of northern summer stationary waves in a GCM, J. Atmos. Sci., 51, 3286–3308, 1994. 5218

Toracinta, E. R., Oglesby, R. J., and Bromwich, D. H.: Atmospheric response to modified CLIMAP ocean boundary conditions during the last glacial maximum, J. Climate, 17, 504–522, 2004. 5208

Ullman, D. J., LeGrande, A. N., Carlson, A. E., Anslow, F. S., and Licciardi, J. M.: Assessing the impact of Laurentide Ice Sheet topography on glacial climate, Clim. Past, 10, 487–507, doi:10.5194/cp-10-487-2014, 2014. 5206, 5207, 5213

Vallis, G. K.: Atmospheric and Oceanic Fluid Dynamics: Fundamentals and Large-Scale Circulation, Cambridge University Press, Cambridge, 2006. 5219

Van Den Berg, J., van de Wal, R., and Oerlemans, H.: A mass balance model for the Eurasian Ice Sheet for the last 120,000 years, Global Planet. Change, 61, 194–208, 2008. 5206

Van der Veen, C. J.: Fundamentals of Glacier Dynamics, CRC Press, London, New York, 2013. 5209

Weber, S. L., Drijfhout, S. S., Abe-Ouchi, A., Crucifix, M., Eby, M., Ganopolski, A., Murakami, S., Otto-Bliesner, B., and Peltier, W. R.: The modern and glacial overturning circulation in the Atlantic ocean in PMIP coupled model simulations, Clim. Past, 3, 51–64, doi:10.5194/cp-3-51-2007, 2007. 5217, 5220

Weertman, J.: The theory of glacier sliding, J. Glaciol., 5, 287–303, 1964. 5209

Zweck, C. and Huybrechts, P.: Modeling of the northern hemisphere ice sheets during the last glacial cycle and glaciological sensitivity, J. Geophys. Res.: Atmos. (1984–2012), 110, D07103, doi:10.1029/2004JD005489, 2005. 5205

CPD
11, 5203–5241, 2015

Table 1. Top of the atmosphere insolation during the northern summer solstice (60° N; Berger and Loutre, 1991) and greenhouse gas concentrations (Petit et al., 1999; Spahni et al., 2005) in the glacial simulations.

	Insolation	CO_2	CH_4	N_2O
MIS5b	505 $W m^{-2}$	210 ppm	450 ppb	240 ppb
MIS4	490 $W m^{-2}$	195 ppm	460 ppb	215 ppb
LGM	480 $W m^{-2}$	185 ppm	350 ppb	200 ppb

CPD
11, 5203–5241, 2015

Table 2. Average summer (JJA) temperature in the Northern Hemisphere $\overline{T}_{NH}$, in Eurasia $\overline{T}_{EA}$ (average within the area 20° W, 180° E, 45° N and 90° N), and the average latitude of the zero-degree isotherm $\overline{\phi}_0$ in the PI OHT simulations.

	$\overline{T}_{NH}$	$\overline{T}_{EA}$	$\overline{\phi}_0$
Present-day	21.1 °C	11.4 °C	75° N
MIS5b PDoro	18.3 °C	9.8 °C	76° N
MIS5b EAonly	18.1 °C	9.5 °C	73° N
MIS5b fullGlacial	17.5 °C	9.2 °C	71° N
MIS4 PDoro	17.3 °C	7.3 °C	71° N
MIS4 EAonly	17.0 °C	6.2 °C	67° N
MIS4 fullGlacial	16.3 °C	5.3 °C	64° N
LGM PDoro	16.3 °C	6.6 °C	70° N
LGM EAonly	15.9 °C	4.5 °C	66° N
LGM fullGlacial	14.0 °C	3.7 °C	57° N

CPD
11, 5203–5241, 2015

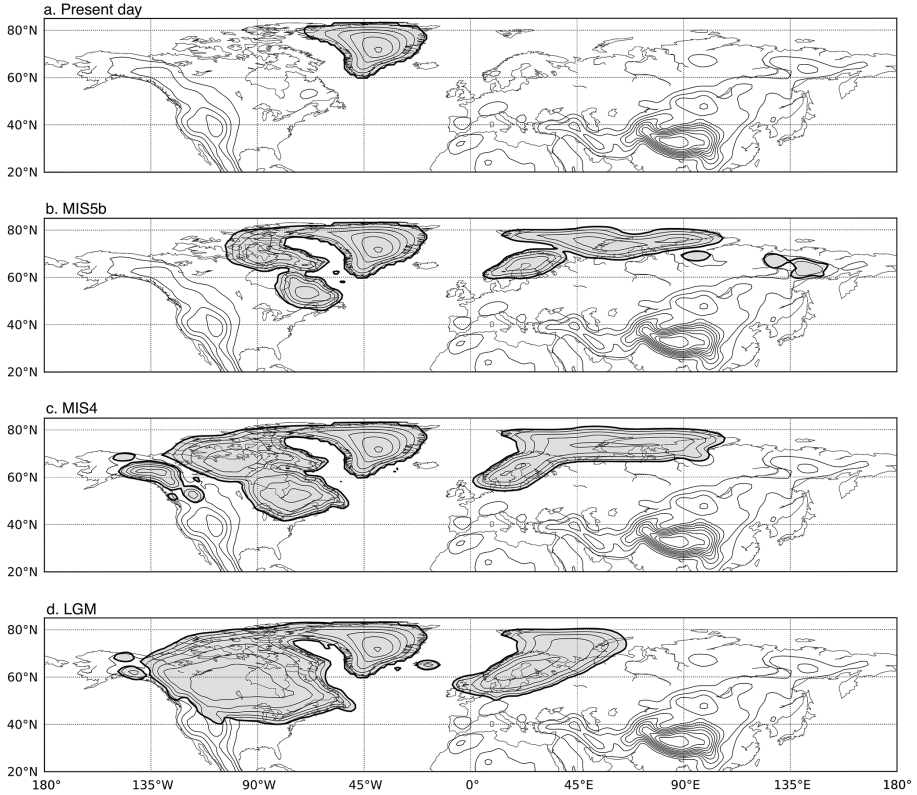

Figure 1. Northern Hemisphere topography representative for **(a)** present-day, **(b)** MIS5b, **(c)** MIS4 and **(d)** LGM, based on the ice-sheet reconstructions in Kleman et al. (2013). The shading represents ice sheets and the contour interval is 500 m.

CPD
11, 5203–5241, 2015

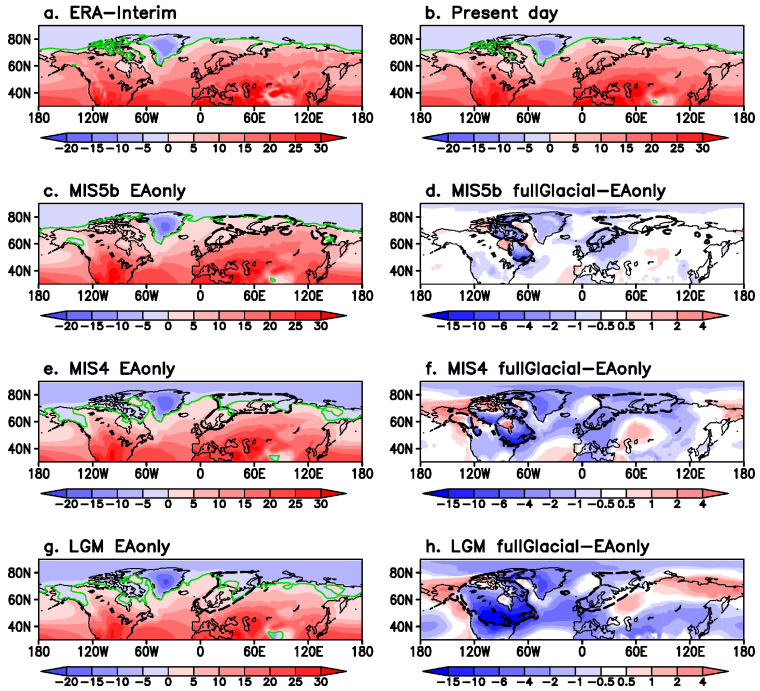

Figure 2. Boreal summer (JJA) surface temperature (in ˚C) from **(a)** the ERA-Interim climatology (Dee et al., 2011), **(b)** the present-day simulation, and the EAonly simulations (with PI OHT) of **(c)** MIS5b, **(e)** MIS4 and **(g)** LGM. The position of the zero-degree isotherm is depicted by the green contour. The JJA surface temperature anomalies induced by North American ice sheet (the difference between the fullGlacial and EAonly simulations; in ˚C) are shown in **(d, f, h)** for **(d)** MIS5b, **(f)** MIS4 and **(h)** LGM. The temperature in the glacial simulations **(c–h)** has been projected to the present-day orography using the standard lapse rate ($\gamma = -6.5 \times 10^{-3}\,\mathrm{K\,m^{-1}}$). The dashed black contours depict the outlines of the Kleman et al. (2013) ice-sheet reconstructions in Eurasia and North America.

CPD
11, 5203–5241, 2015

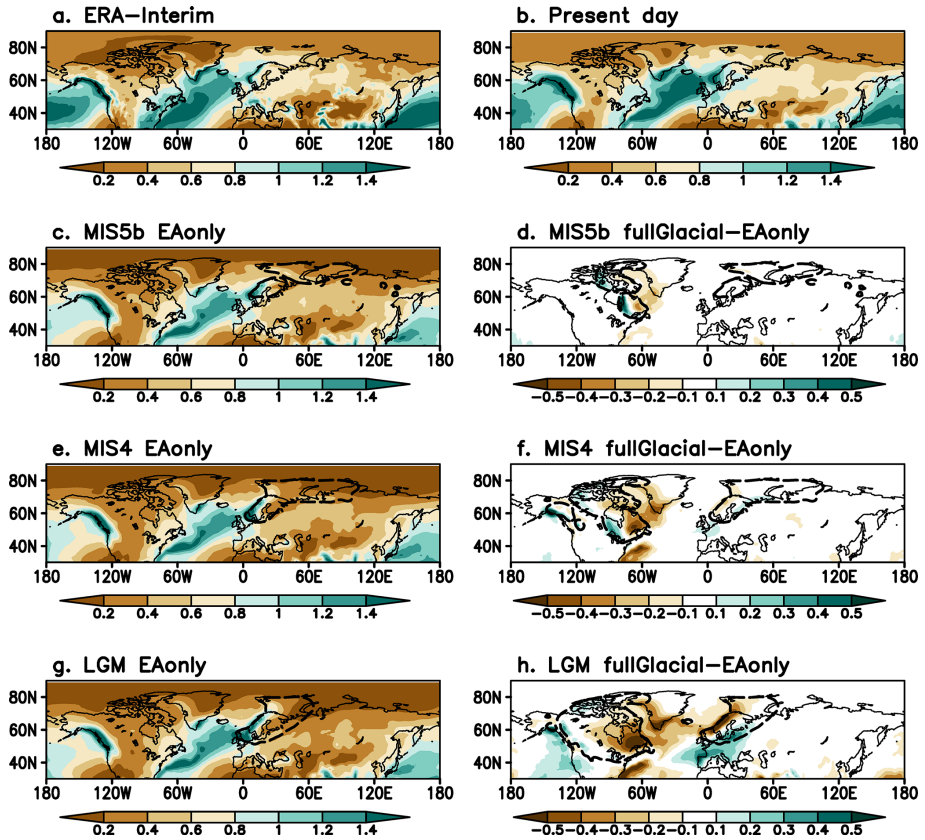

Figure 3. Annual precipitation (in m) from **(a)** the ERA-Interim climatology (Dee et al., 2011), **(b)** the present-day simulation, and the EAonly simulations (with PI OHT) of **(c)** MIS5b, **(e)** MIS4 and **(g)** LGM. The annual precipitation anomalies induced by North American ice sheet (the difference between the fullGlacial and EAonly simulations; in m) are shown in **(d, f, h)** for **(d)** MIS5b, **(f)** MIS4 and **(h)** LGM. The dashed black contours depict the outlines of the Kleman et al. (2013) ice-sheet reconstructions in Eurasia and North America.

CPD
11, 5203–5241, 2015

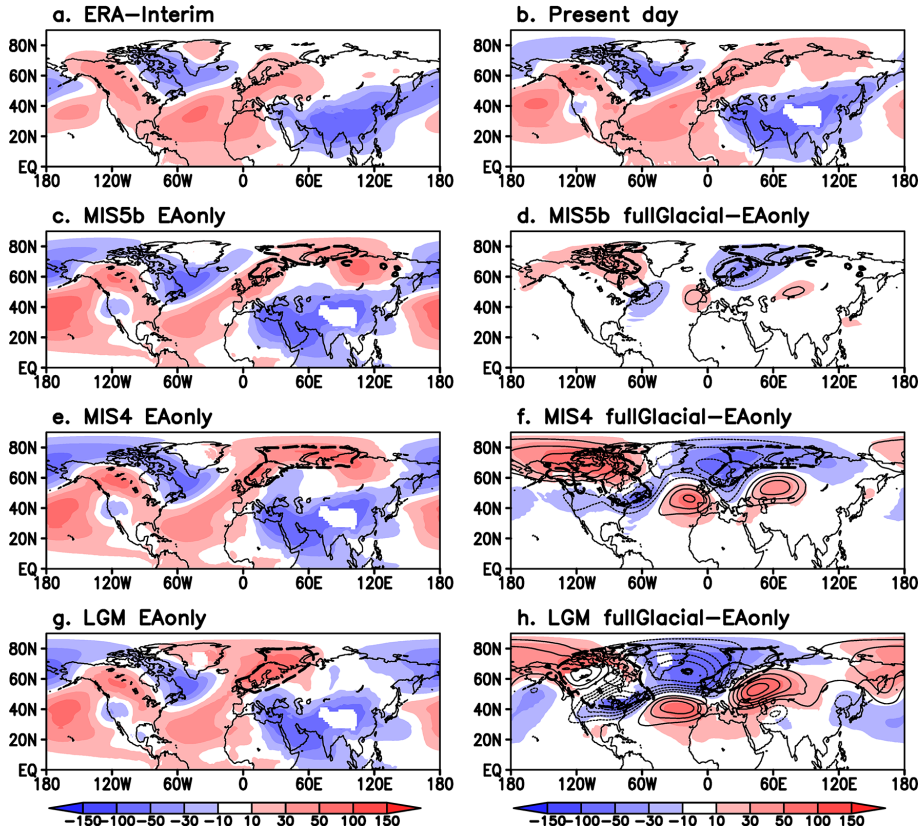

Figure 4. Same as Fig. 3 but for the JJA geopotential height anomalies (in m; zonal mean subtracted) at 700 hPa (shading) and 300 hPa (black contours in **d**, **f**, **h**; contour interval is 30 m, and negative values are dashed). Positive anomalies refer to anticyclonic circulation, and negative anomalies to cyclonic circulation.

CPD
11, 5203–5241, 2015

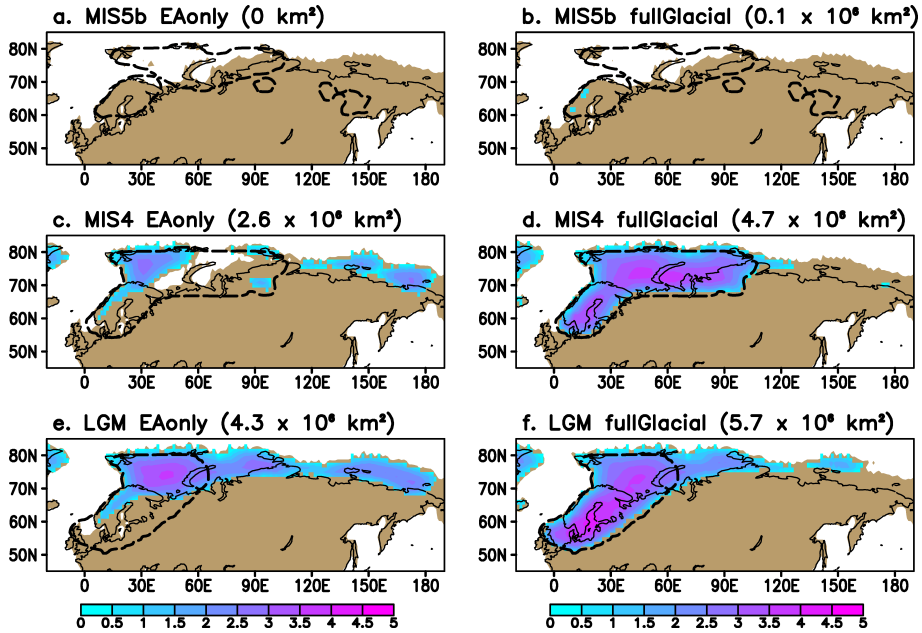

Figure 5. Simulated equilibrium ice thickness in Eurasia (shading; in km) using the PI OHT climate forcing from the EAonly **(a, c, e)** and fullGlacial **(b, d, f)** simulations for MIS5b **(a, b)**, MIS4 **(c, d)** and LGM **(e, f)**. The dashed black contours depict the outlines of the Kleman et al. (2013) ice-sheet reconstructions. The land area in the simulations is indicated by the brown color, and the present-day coastline by the thin black contour. The total Eurasian ice-sheet area in each simulation is indicated in the panel titles.

CPD
11, 5203–5241, 2015

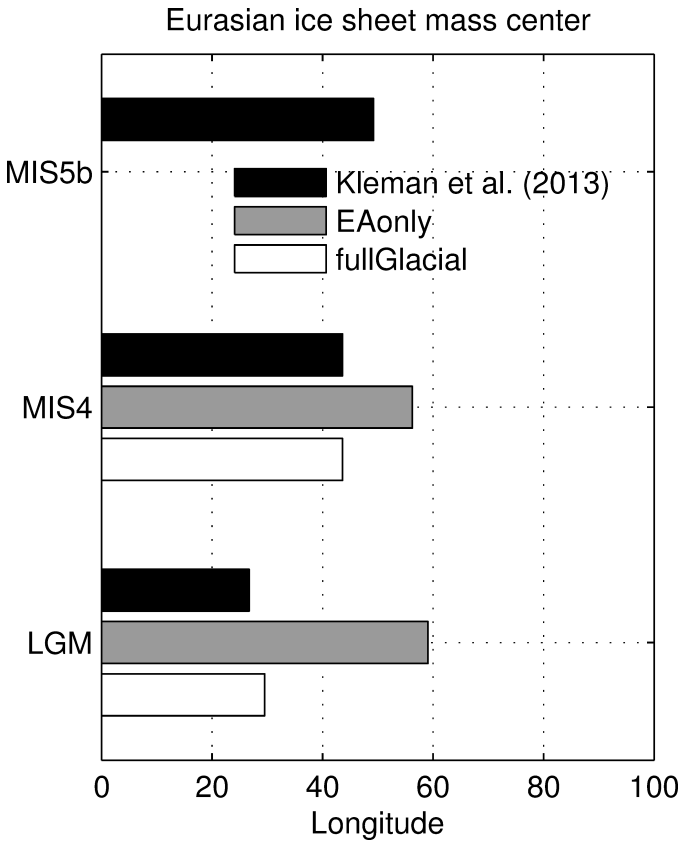

Figure 6. The longitude of the center of mass of the Eurasian ice sheet (λ_c) in the Kleman et al. (2013) reconstructions (black bars), EAonly simulations (gray bars), and fullGlacial simulations (white bars).

CPD
11, 5203–5241, 2015

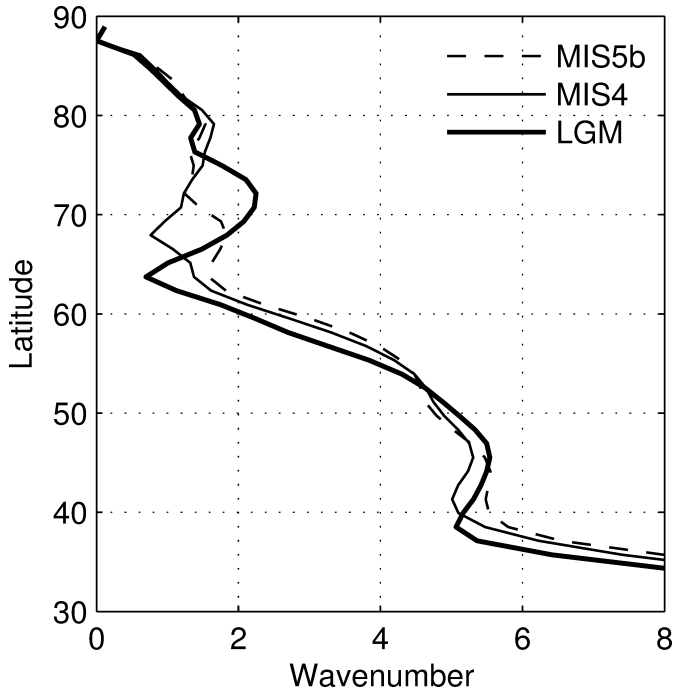

Figure 7. The stationary wavenumber K_s (Eq. 5) calculated using the JJA climatology of the zonal-mean zonal wind at 300 hPa from the MIS5b (dashed line), MIS4 (thin solid line) and LGM (thick solid line) EAonly simulations.

CPD
11, 5203–5241, 2015

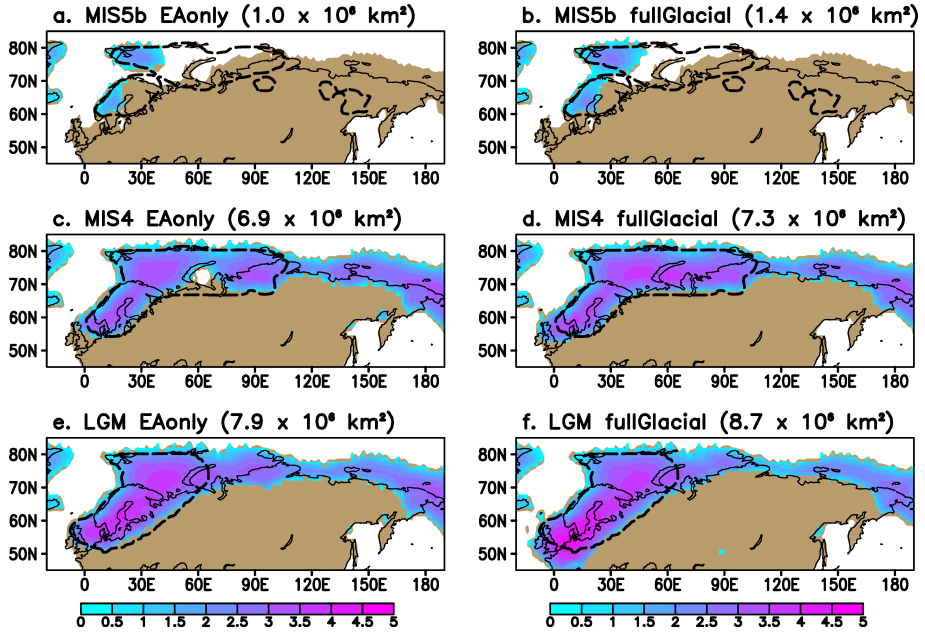

Figure 8. Same as Fig. 5 but using the climate forcing from the atmospheric simulations with LGM OHT.

CPD
11, 5203–5241, 2015

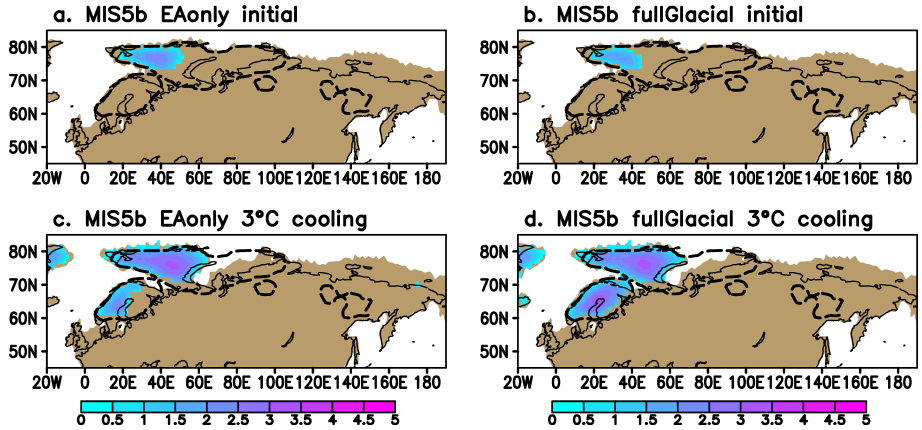

Figure 9. Simulated equilibrium ice thickness in Eurasia (shading; in km) using the MIS5b (with PI OHT) climate forcing from the EAonly **(a, c)** and fullGlacial **(b, d)** simulations. In **(a, b)**, the simulations were initialized with the reconstructed ice-sheet topography from Kleman et al. (2013), and in **(c, d)** the JJA surface temperature was reduced by 3 °C throughout the entire simulation.

CPD
11, 5203–5241, 2015